Templated fabrication of nanostructured Ni brush for hydrogen evolution reaction

Sheng-Chieh Lin, Yu-Fan Chiu, Pu-Wei Wu,[a] Yi-Fan Hsieh, and Cheng-Yeou Wu
Department of Materials Science and Engineering, National Chiao Tung University, Hsin-chu 300, Taiwan, Republic of China

(Received 31 January 2010; accepted 10 June 2010)

We fabricated a nanostructured brush by carrying out Ni deposition on a through-channel anodic aluminum oxide (AAO) template, followed by removal of the AAO skeleton. The AAO was prepared by a two-step anodization process resulting in pore diameter and thickness of 350 nm and 40 μm, respectively. Subsequently, the AAO underwent an electroless deposition involving sensitization, activation, and Ni plating, in conjunction with polyethylene glycol used as the inhibitor to prevent premature closing of pore opening. After deliberate control in relevant parameters, we obtained a conformal Ni overcoat along every pore channel leading to a reduced average pore diameter of 78 nm. Afterward, the sample was immersed in a KOH solution to remove the AAO structure, forming freestanding Ni tubules in a brush configuration. The nanostructured brush revealed considerable enhancement for hydrogen evolution reaction in both current-potential polarization and galvanostatic measurements, which were attributed to the increment in apparent surface area.

I. INTRODUCTION

Preparation of nanostructured materials using an anodic aluminum oxide (AAO) template has received considerable attention recently for possible applications in optics, electronics, batteries, and biosensing.[1–4] For example, metals, oxides, and polymers in nanowires or nanodots have been successfully fabricated with impressive results.[5–8] Formed by anodization of Al in an acidic electrolyte, the AAO revealed perpendicular pore channels in adjustable pore diameters and densities contingent on the type of acid, temperature, and voltage involved during the anodization process.[9,10] Unfortunately, due to its insulating nature, templated synthesis using the AAO structure is limited to electroless approaches such as sol-gel, chemical conversion, electroless plating, and physical vapor deposition.[11–14] Among them, the electroless plating route is considered to be the most versatile one because it entails a relatively simple setup to produce a rich variety of deposits.[15,16]

Metallization of AAO is a field of few studies but its successful demonstration is expected to enable the synthesis of new materials for novel applications. To fabricate a conductive AAO, a conformal metal deposition is necessary on every pore channel without clogging the pore opening prematurely. This is especially challenging as the aspect ratio for these pore channels is typically in the range of 50 to 200. Therefore, a practical solution is to adopt an electroless formulation in conjunction with suitable inhibitors. For the past 10 years, extensive efforts have been devoted to electroplate Cu in submicronmeter trenches for damascence structure.[17–19] Among many additives explored, polyethylene glycol (PEG) is a popular inhibitor to retard Cu deposition because it easily adsorbs on the active sites of the substrate.[20] Since the electroless Cu deposition is often performed in an alkaline electrolyte, which is corrosive for the AAO template, we selected an alternative Ni deposition to metallize the AAO with the presence of PEG as the additive. We realize that a freestanding Ni tubular array can be formed once the metallization is completed and removal of the AAO skeleton is successful. These Ni tubules might be useful as a substrate to promote desirable catalytic reactions because of its excessive surface area.

Previously, Ni with increased surface area (Raney Ni) was designed and tested for hydrogen evolution reaction (HER) in an alkaline electrolyte.[21–23] The HER is a critical reaction to produce hydrogen fuel from water electrolysis, which involves an electrochemical process to decompose water under a sufficient external voltage. To expedite the HER, noble metals such as Pt and Mo are used as the electrocatalysts.[24,25] However, for large-scaled economic production of hydrogen, the Ni and its alloys are widely used as the electrode materials.

In this work, we demonstrated the fabrication of freestanding Ni tubules by performing electroless deposition

[a]Address all correspondence to this author.
e-mail: ppwu@mail.nctu.edu.tw
DOI: 10.1557/JMR.2010.0248

on a through-channel AAO template, followed by chemical removal of the AAO skeleton. This nanostructured Ni array was shown to render a larger catalytic ability for the HER as opposed to a planar electrode.

II. EXPERIMENTAL

The nanostructured Ni array was fabricated via a templated synthetic route on a through-channel AAO substrate. To prepare the through-channel AAO template, an Al foil (99.5% purity) in a radius of 14 and 0.2 mm thickness was used. First, the as-received Al foil underwent pretreatments including Ar annealing and electropolishing. Next, the sample was subjected to a two-step anodization process to produce well-aligned pore channels. During the first anodization, irregular pores were formed on the Al surface. Those random pores were subsequently removed to leave a surface vestige. Afterward, the second anodization was performed to develop vertical pore channels. Next, the unreacted Al on the backside was chemically removed to expose the Al_2O_3 barrier layer at the channel bottom. Finally, the Al_2O_3 barrier layer was etched open, producing the through-channel AAO template in a radius of 11 mm.

To metallize the through-channel AAO template, an electroless plating of Ni was carried out in which multiple steps of sensitization and activation were used, followed by Ni deposition. Because the AAO template was unstable in an alkaline solution, we chose an acidic bath instead. The sample was first immersed in a sensitizing solution to allow adequate adsorption of Sn^{2+}. After rinsing with deionized water, the AAO template was dipped into an activation solution to initiate spontaneous oxidation of Sn^{2+} into Sn^{4+}, and reduction of Pd^{2+} to form nanocrystalline Pd. These Pd nanocrystallites would act as the catalytic centers for subsequent Ni^{2+} reduction and growth. This process of sensitization and activation was repeated five times to reach a desirable Pd coverage. For Ni formulation, $NiSO_4 \cdot 6H_2O$ was used as the metal source and NaH_2PO_2 was used as the reducing agent. NaOH was used to adjust the pH value of the plating formulation. In addition, chemicals including PEG (Mw = 2000) and Pb^{2+} were added as the inhibitor. Finally, the sample was immersed in a KOH solution to remove the embedded AAO skeleton, leading to the formation of freestanding Ni tubules in a brush configuration. A schematic for the fabrication steps involved is presented in Fig. 1. Relevant processing parameters and formulation in each step are listed in Table I.

In electrochemical analysis, a three-electrode arrangement was adopted where the reference and counter electrodes were Ag/AgCl and Pt foil (5.7 cm^2), respectively. The nanostructured Ni brush (1 cm^2) was fastened by a Teflon (DuPont, Wilmington, DE) holder serving as the

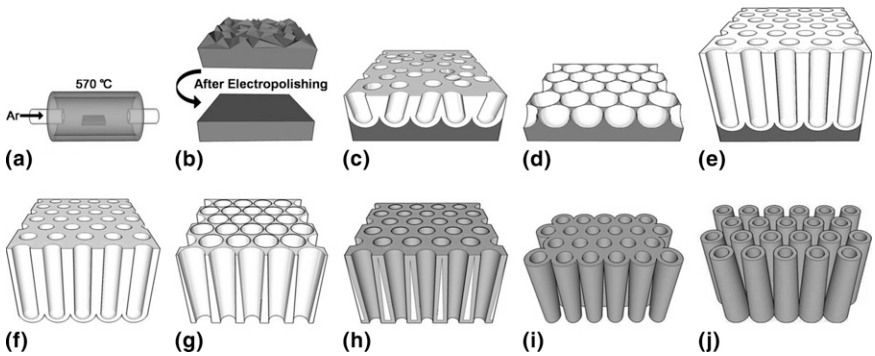

FIG. 1. Schematic diagrams for the processing steps involved in the fabrication of the nanostructured Ni brush; (a) annealing, (b) electropolishing, (c) first anodization, (d) removal of surface oxide, (e) second anodization, (f) removal of backside Al, (g) removal of barrier layer, (h) Ni deposition, (i) nanostructured brush in top view, and (j) nanostructured brush in bottom view.

TABLE I. Processing parameters and formulation used in the fabrication of nanostructured Ni brush.

Electropolishing	$HClO_4$, $C_4H_9OCH_2CH_2OH$, and C_2H_5OH (15:15:70 vol%) at 10 °C and 35 V for 10 min
First anodization	0.3 M H_3PO_4 at 170 V and 0 °C for 30 min
Surface oxide removal	1.8 wt% CrO_3 and 6 wt% H_3PO_4 at 60 °C for 40 min
Second anodization	0.3 M H_3PO_4 at 170 V and 0 °C for 13 h
Backside Al removal	100 mL HCl, 100 mL H_2O, and 3.4 g $CuCl_2$ at 26 °C for 5 min
Barrier layer removal	5 wt% H_3PO_4 at 40 °C for 2 h
Sensitization	0.3 wt% $SnCl_2$ and 2.5 wt% HCl at 26 °C for 1 min
Activation	0.1 wt% $PdCl_2$ and 1 wt% HCl at 26 °C for 1 min
Electroless deposition	20 g/L $NiSO_4$, 25 g/L NaH_2PO_2, 2 ppm $Pb(NO_3)_2$, and 500 ppm PEG (Mw. 2000) in pH 5 and 70 °C for 1 h
AAO removal	1 M KOH at 26 °C for 10 min

working electrode. Current-potential polarizations (i–V) were conducted by EG&G 263A (Oak Ridge, TN) in 1 M KOH solution at a scan rate of 5 mV/s for −0.2 to −1.5 V. Galvanostatic profiles were also obtained at 30 mA/cm^2 to determine the lifetime performance for HER. For comparison purposes, we followed identical steps to deposit Ni electrolessly on a Cu-coated Si substrate and evaluated its i–V and life time characteristics. We selected the Cu-coated Si substrate to prepare the planar Ni plate because it provided a relatively smooth surface for Ni–P deposition. In addition, to minimize possible interferences from the Si substrate in electrochemical measurements, the contact was made through the Ni–P layer directly.

Morphologies for the nanostructured Ni brush were observed via a field-emission scanning electron microscopy (FE-SEM; JEOL-JSM-6500F, Tokyo, Japan). Chemical composition and phase of the Ni deposit were determined by energy-dispersive x-ray analysis (EDX) and x-ray diffraction (XRD; MAC MXP18, Tokyo, Japan), respectively. Capillary flow porometer was used to validate the through-channel pores in the AAO template and their size distribution before and after Ni deposition. The electrical resistance for the metallized AAO was obtained by a four-point measurement (Keithley 2000, Cleveland, OH) in the through-channel direction.

III. RESULTS AND DISCUSSION

We fabricated the through-channel AAO template with a radius of 11 mm and 40 μm thickness. Its pore opening was 350 nm, resulting in an aspect ratio of 114. Since the template was open at both sides, its effective aspect ratio became 57. Therefore, our objective of conformal Ni deposition within every pore channel without closing their pore openings was rather formidable. Previously, we demonstrated the conformal deposition of Ni on an AAO substrate of 10 μm thickness with an aspect ratio of 20.[26] Because of its reduced thickness, the sample became extremely brittle. Mechanical properties can be improved simply by increasing the thickness, which amounts to a larger aspect ratio. Notably, current Cu damascence process entails the preparation of Cu seed layers conformally in trenches with aspect ratios of 3 to ~5 but the deposition at pores with higher aspect ratios is still lacking.[27,28]

Since the AAO template was not conductive, electroless Ni deposition required the proper seeding of Pd to provide adequate nucleation sites. It is understood that the formation of Ni initiates at the Pd nuclei that grows into larger nodules. At a later stage, these nodules are sufficiently large to contact each other and form a continuous film. Therefore, to obtain conformal Ni deposition, a desirable Pd seeding is necessary. Figure 2 provides the SEM images for the Ni nodules formed on the Pd nuclei in sensitization and activation of one, three, and five times, respectively. As shown in Figs. 2(a) and 2(b), sensitization and activation for single and three times lead to Pd nuclei densities of 5.8×10^{10}/cm^2 and 7.1×10^{10}/cm^2, respectively. The Pd density was increased to 8.6×10^{10}/cm^2 after five repeated steps of sensitization and activation, as shown in Fig. 2(c). This corresponded to a Pd–Pd distance of 34.1 nm. Assuming a three-dimensional Ni growth, a conformal Ni film could be realized at a minimum thickness of 17 nm.

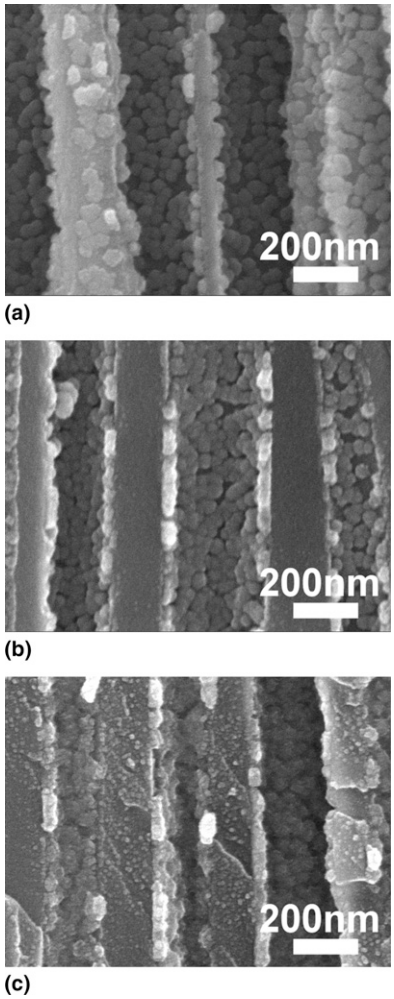

FIG. 2. SEM images of Ni nodules after sensitization and activation for (a) one, (b) three, and (c) five times, and followed by 5 min Ni electroless plating.

Figure 3 provides the top and cross-sectional SEM images for the AAO after conformal Ni deposition. As shown in Fig. 3(a), there was Ni deposit within every pore channel but its amount at the pore opening was relatively subdued. Apparently, the diameter for the pore opening on surface was reduced to 250 nm from 350 nm. Formation of Ni tubule inside the AAO pore channel was clearly visible from Figs. 3(b) and 3(c) in cross-sectional views. Individual pore channel was covered by a conformal Ni deposit and its thickness was estimated to be 60–80 nm.

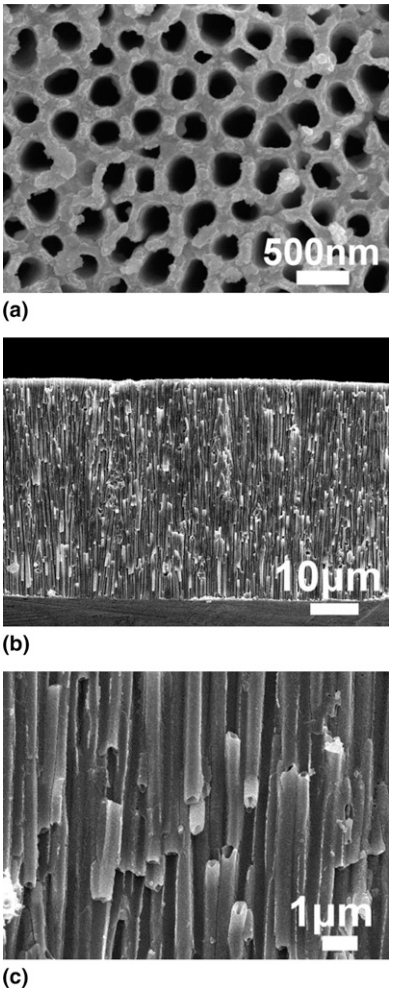

FIG. 3. SEM images of AAO after conformal Ni deposition in (a) top view, (b) cross-sectional view in low magnification, and (c) cross-sectional view in large magnification.

Notably, the Ni deposit appeared uniform without defects and uncovered area. It can be seen that the deposit on the pore opening was considerably less as opposed to that within the pore channels. This unique character was attributed to the PEG inhibitor that preferentially adsorbed on the surface but slow in diffusion into the pore channels.

After Ni deposition, the transparent AAO template darkened considerably. The result from XRD for the metallized AAO is presented in Fig. 4. Due to the interference of amorphous AAO signals; there were substantial noises in the diffraction pattern. Nevertheless, we observed a broad Ni (111) peak at 44.5°. This confirmed that the Ni deposit was nanocrystalline in nature. Analysis from EDX indicated that the Ni deposit contained 15.34 wt% of phosphorus. This amount of phosphorus was not unexpected because earlier literature has established that electroless Ni deposition in an acidic electrolyte always includes the phosphorus as a codeposit and its amount is inversely proportional to the deposition rate.[29] Previous work has demonstrated that the amount

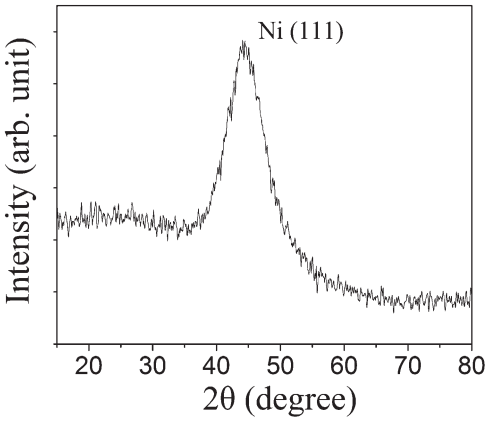

FIG. 4. XRD pattern for the AAO after conformal Ni deposition.

of P in Ni–P would affect the HER catalytic ability. For example, there appears to be an optimized composition range of P that leads to HER enhancement over samples of pure Ni.[30,31] In electroless Ni–P deposition, the amount of P is determined by variables such as additives, pH, and deposition temperature. The effect of substrate on the resulting Ni–P composition is considered negligible. Accordingly, the Ni–P composition on the planar Ni plate was 15.66 wt%. This minor difference was not likely to produce noticeable difference in HER ability. Hence, the HER measurements we obtained were primarily attributed to the effect of surface area.

Direct validation of through-channel characteristics for the Ni-plated AAO can be obtained by porometer measurements. Figure 5 presents the relevant pore size and distribution for the AAO template before and after Ni deposition. In general, results from the porometer measurements represented the most constricted regime within the pore channels and hence their reading was typically much smaller than direct SEM observations. From Fig. 3(a), the majority of the through-channel pores on the AAO template revealed an average diameter of 202 nm. After Ni deposition, their values were significantly reduced to 78 nm. Obviously, the Ni deposition helped in reducing pore channel inhomogeneity.

A direct electrical conductivity measurement was used to confirm uniform coverage of Ni on every AAO pore channel. We applied two Cu pads on both surfaces of the metallized AAO and recorded the resulting resistance value. Prior to Ni deposition, the resistance for the AAO template was above 10^6 Ω. After Ni deposition, its value was reduced to 0.18 Ω. This outcome validated the conductive nature of the metallized AAO.

Since there existed a slight difference in the AAO pore size from both sides, more Ni plating was observed on the top surface. As a result, after KOH etching the additional Ni would act as a substrate anchoring individual tubules. Figure 6 provides the SEM images for the nanostructured Ni brush. As shown in Fig. 6(a), without

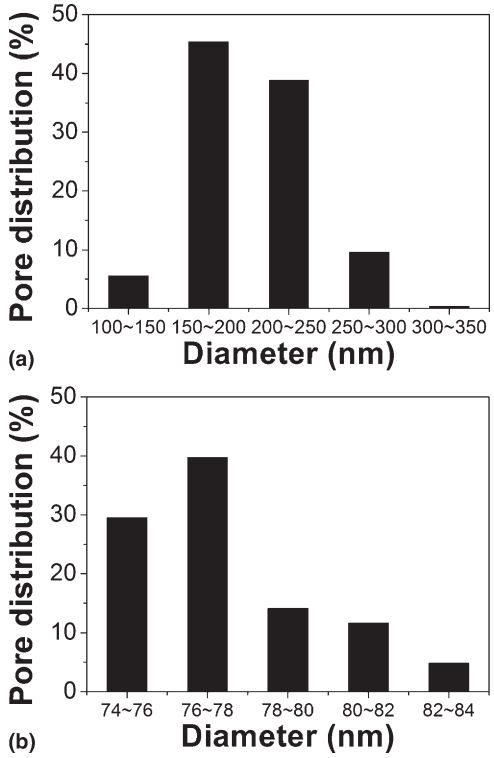

FIG. 5. Size and distribution of the pore channels for the AAO template (a) before, and (b) after conformal Ni deposition.

AAO supports individual Ni tubules were clearly distinguishable. Figures 6(b) and 6(c) present the SEM images from bottom and top views. Apparently, these freestanding Ni tubules revealed a considerable structural stability and their size uniformity was relatively consistent. At this stage, these samples demonstrated moderate flexibility unlike that of AAO and metallized AAO, which were rigid and brittle. These freestanding Ni tubular arrays are expected to introduce many applications because of their excessive surface area and conductive nature.

Figure 7 exhibits the HER *i*–*V* profiles for the nanostructured Ni brush and planar Ni plate. In an alkaline solution, the open circuit potential for both samples was −0.2 V (versus Ag/AgCl). Once a reducing overpotential was imposed, we started to record current responses when the potential reached −0.9 V. Apparently, the nanostructured Ni brush demonstrated a larger HER current as opposed to that of planar Ni plate. Since the electrochemical reaction is known to be proportional to the electrode surface area, and samples here possessed a notable difference in the apparent surface area, further deliberation on the effective current densities becomes warranted. The actual surface area for the nanostructured Ni brush could be estimated by the following equation:

$$A = \rho \times t \times (2\pi R + 2\pi r) \quad , \qquad (1)$$

where A is the actual surface area, ρ is the number of the Ni tubules in 1 cm^2 geometrical footprint, t is the tubular

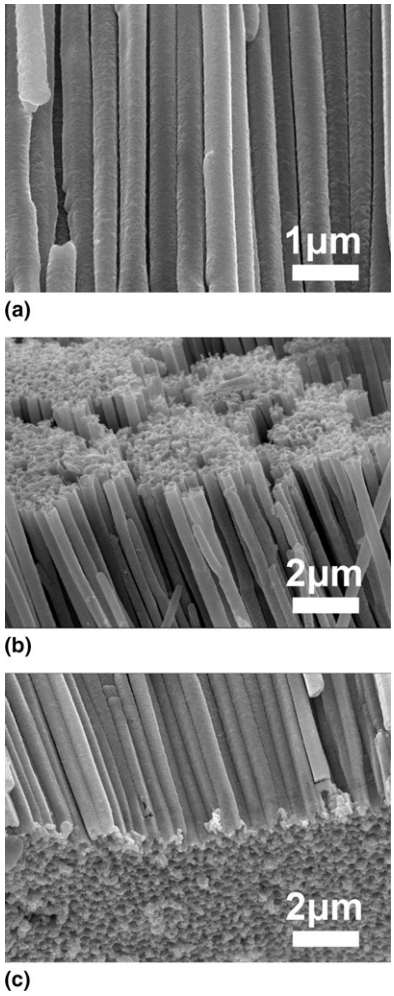

FIG. 6. SEM images for the nanostructured Ni brush in (a) middle view, (b) bottom view, and (c) top view.

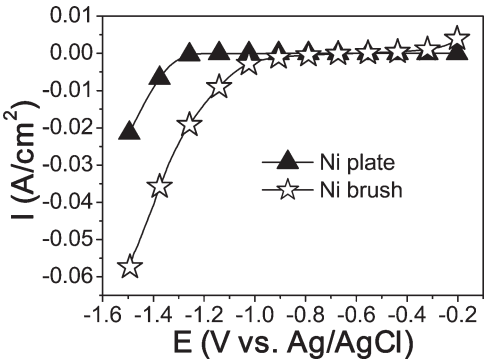

FIG. 7. HER current-potential profiles for the nanostructured Ni brush and planar Ni plate, respectively.

height, and R and r are the outer and inner radius of the Ni tubules. The values for ρ, t, R, and r were 6.3 × 10^8/cm^2, 4 × 10^4 nm, 101 nm, and 39 nm, respectively. Table II provides the comparison for the actual surface area and effective current densities at selective potentials

TABLE II. Values for apparent and effective current densities for the nanostructured Ni brush and planar Ni plate at selective potentials.

		−1.3 V		−1.5 V	
Sample	Surface area (cm^2)	Apparent current (mA/cm^2)	Effective current (mA/cm^2)	Apparent current (mA/cm^2)	Effective current (mA/cm^2)
Planar Ni plate	1	1.68	1.68	22.2	22.2
Nanostructured Ni brush	211	24.3	0.12	58.6	0.28

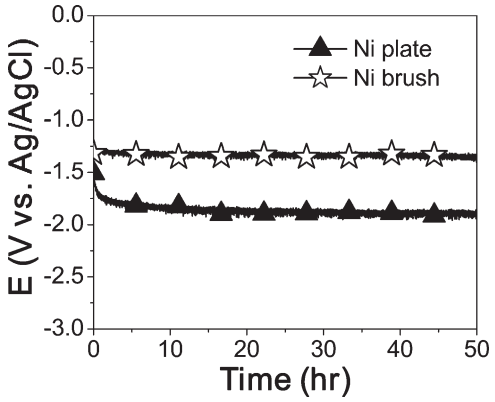

FIG. 8. Galvanostatic HER profiles for the nanostructured Ni brush and planar Ni plate, respectively.

for the nanostructured Ni brush and planar Ni plate. Unfortunately, the effective current densities for the nanostructured Ni brush were substantially smaller than those of planar Ni plate. This suggested that the area responsible for the HER in the nanostructured Ni brush was relatively subdued. This reduction in useful area was caused by the limitation of mass transport within individual Ni tubule and between them. It is realized that during HER, the freshly produced hydrogen might be entrapped and interrupted with electrolyte inflow. This behavior was likely to be particularly pronounced since the nanotubular structure only allowed vertical bubble escapes. Moreover, according to the literature the trapped gas bubbles were expected to engender substantial ohmic resistance in the electrolyte that often resulted in loss of catalytic ability.[32,33] Therefore, we understood that the effective surface area for the HER was confined primarily within the top portion of the Ni tubules. Similar results were recently reported on the compromised performance in nanostructured electrodes for water electrolysis.[34,35]

The HER *i–V* measurement provides transient characteristics for quick catalytic evaluations. To further confirm the applicability of nanostructured Ni brush, it is necessary to explore its galvanostatic behavior for lifetime determination. Figure 8 presents the voltage profiles for the nanostructured Ni brush and planar Ni plate, respectively. Both profiles revealed rather flat response with voltage plateaus of −1.34 and −1.86 V, respectively. These values were slightly lower than what we expected from earlier *i–V* curves. However, both voltage profiles indicated the electrode structures were not severely damaged after release of gas bubbles.

So far, we demonstrated the fabrication of nanostructured Ni tubules at a high aspect ratio and evaluated their applicability for HER activities. Since both nanostructured Ni and planar Ni demonstrated similar composition and phase, the distinction in HER ability was attributed entirely to their surface area difference. We realized that further improvements in current characteristics require the optimization of size and crystal structure of the NI nanostructured brush.

IV. CONCLUSIONS

A through-channel AAO substrate with an average pore diameter of 350 nm and 40 μm thickness was used as the template to fabricate a nanostructured Ni tubular array. This was achieved via an electroless Ni conformal deposition on every pore channel with PEG as the inhibitor, followed by chemical removal of the AAO skeleton. The Ni tubular array exhibited impressive structural integrity with a pore opening of 78 nm, and one side was anchored on the Ni in a brush configuration. In comparison with a planar Ni plate, the nanostructured Ni brush demonstrated a larger current response for the HER in both *i–V* polarizations and galvanostatic measurements. This improvement in current characteristics was due to the increment in surface area in the nanostructured electrode.

ACKNOWLEDGMENTS

The authors would like to express their gratitude to Professor Pang Lin and George Tu for their assistance in laboratory equipment and space.

REFERENCES

1. J.B. Shi, Y.C. Chen, C.W. Lee, Y.T. Lin, and C. Chen: Optical and magnetic properties of 30 and 60 nm Ni nanowires. *Mater. Lett.* **62,** 15 (2008).
2. P.L. Chen, W.J. Huang, J.K. Chang, C.T. Kuo, and F.M. Pan: Fabrication and field-emission characteristics of highly ordered titanium oxide nanodot arrays. *Electrochem. Solid-State Lett.* **8,** H83 (2005).
3. J.H. Kim, T. Ayalasomayajula, V. Gona, and D. Choi: Fabrication and electrochemical characterization of a vertical array of MnO_2 nanowires grown on silicon substrates as a cathode material for lithium rechargeable batteries. *J. Power Sources* **183,** 366 (2008).

4. J. Yuan, K. Wang, and X. Xia: Highly ordered platinum-nanotubule arrays for amperometric glucose sensing. *Adv. Funct. Mater.* **15,** 803 (2005).
5. A.W. Zhao, C.H. Ye, G.W. Meng, L.D. Zhang, and P.M. Ajayan: Tellurium nanowire arrays synthesized by electrochemical and electrophoretic deposition. *J. Mater. Res.* **18,** 2318 (2003).
6. J. Zhang, J.E. Kielbasa, and D.L. Carroll: Nanostructure of the nanopores in anodic aluminum oxide films used as template to fabricate Ag nanowires. *J. Mater. Res.* **24,** 1735 (2009).
7. C.J. Yang, C. Chen, P.W. Wu, J.M. Shieh, S.M. Wang, and S.W. Liang: Fabrication of ordered Ta_2O_5 nanodots using an anodic aluminum oxide template on Si substrate. *J. Mater. Res.* **22,** 1064 (2007).
8. X. She, G. Song, J. Li, P. Han, S. Yang, and Z. Peng: Preparation and characterization of polyamide 66 nanotubes and nanowires on an anodic aluminum oxide template by a physical wetting method. *J. Mater. Res.* **21,** 1209 (2006).
9. G.E. Thompson and G.C. Wood: Porous anodic film formation on aluminum. *Nature* **290,** 230 (1981).
10. A.P. Li, F. Müller, A. Birner, K. Nielsch, and U. Gösele: Polycrystalline nanopore arrays with hexagonal ordering on aluminum. *J. Appl. Phys.* **84,** 6023 (1999).
11. Y. Yuan, C. Liu, Y. Zhang, and X. Shan: Sol-gel auto-combustion synthesis of hydroxyapatite nanotubes array in porous alumina template. *Mater. Chem. Phys.* **112,** 275 (2008).
12. Y.S. Kim, V.P. Godbole, J.H. Cho, G. Khang, and H.S. Shin: Plasma enhanced chemical vapor deposition of palladium in anodic aluminum oxide template. *Curr. Appl. Phys.* **6S1,** e58 (2006).
13. S.H. Zhang, Z.X. Xie, Z.Y. Jiang, X. Xu, J. Xiang, R.B. Huang, and L.S. Zhang: Synthesis of silver nanotubes by electroless deposition in porous anodic aluminum oxide templates. *Chem. Commun. (Camb.)* 1106 (2004).
14. H. Masuda and M. Satoh: Fabrication of gold nanodot array using anodic porous alumina as an evaporation mask. *Jpn. J. Appl. Phys.* **35,** L126 (1996).
15. W. Wang, N. Li, X. Li, W. Geng, and S. Qiu: Synthesis of metallic nanotube arrays in porous aluminum oxide template through electroless deposition. *Mater. Res. Bull.* **41,** 1417 (2006).
16. D. Guo, L. Fan, J. Sang, Y. Liu, S. Huang, and X. Zou: Fabrication of a regular tripod Ni–P nanorod array and an AAO template with regular branched nanopores using a current-controlled branching method. *Nanotechnology* **18,** 405304 (2007).
17. P.C. Andricacos, C. Uzoh, J.O. Dukovic, J. Horkans, and H. Deligianni: Damascene copper electroplating for chip interconnections. *IBM J. Res. Dev.* **42,** 567 (1998).
18. A.C. West, S. Mayer, and J. Reid: A superfilling model that predicts bump formation. *Electrochem. Solid-State Lett.* **4,** C50 (2001).
19. H.C. Tsai, Y.C. Chang, and P.W. Wu: Rapid galvanostatic determination on levelers for superfilling in Cu electroplating. *Electrochem. Solid-State Lett.* **13,** D7 (2010).
20. J.J. Kelly and A.C. West: Copper deposition in the presence of polyethylene glycol II. Electrochemical impedance spectroscopy. *J. Electrochem. Soc.* **145,** 3477 (1998).
21. R.K. Shervedani and A. Lasia: Studies of the hydrogen evolution reaction on Ni–P electrodes. *J. Electrochem. Soc.* **144,** 511 (1997).
22. D.R. Kim, K.W. Cho, Y.I. Choi, and C.J. Park: Fabrication of porous Co–Ni–P catalysts by electrodeposition and their catalytic characteristics for the generation of hydrogen from an alkaline $NaBH_4$ solution. *Int. J. Hydrogen Energy* **34,** 2622 (2009).
23. S.I. Tanaka, N. Hirose, and T. Tanaki: Evaluation of raney-nickel cathodes prepared with aluminum powder and titanium hydride powder. *J. Electrochem. Soc.* **146,** 2477 (1999).
24. J.Y. Huot, M.L. Trudeau, and R. Schulz: Low hydrogen overpotential nanocrystalline Ni–Mo cathodes for alkaline water electrolysis. *J. Electrochem. Soc.* **138,** 1316 (1991).
25. S.A. Grigoriev, P. Millet, and V.N. Fateev: Evaluation of carbon-supported Pt and Pd nanoparticles for the hydrogen evolution reaction in PEM water electrolysers. *J. Power Sources* **177,** 281 (2008).
26. S.C. Lin, C.H. Lai, and P.W. Wu: Conformal deposition of Ni–P on anodic aluminum oxide template. *Electrochem. Solid-State Lett.* **11,** D1 (2008).
27. S.Y. Chang, C.J. Hsu, R.H. Fang, and S.J. Lin: Electrochemical deposition of nanoscaled palladium catalysts for 65 nm copper metallization. *J. Electrochem. Soc.* **150,** C603 (2003).
28. S.Y. Chang, C.W. Lin, H.H. Hsu, J.H. Fang, and S.J. Lin: Integrated electrochemical deposition of copper metallization for ultralarge-scale integrated circuits. *J. Electrochem. Soc.* **151,** C81 (2004).
29. G.F. Cui, N. Li, D.Y. Li, and M.G. Chi: Study of optimized complexing agent for low-phosphors electroless nickel plating bath. *J. Electrochem. Soc.* **152,** C669 (2005).
30. Z.D. Wei, A.Z. Yan, Y.C. Feng, L. Li, C.X. Sun, Z.G. Shao, and P.K. Shen: Study of hydrogen evolution reaction on Ni–P amorphous alloy in the light of experimental and quantum chemistry. *Electrochem. Commun.* **9,** 2709 (2007).
31. A.M. Fundo and L.M. Abrantes: The electrocatalytic behavior of electroless Ni–P alloys. *J. Electroanal. Chem.* **600,** 63 (2007).
32. D. Kiuchi, H. Matsushima, Y. Fukunaka, and K. Kuribayashi: Ohmic resistance measurement of bubble froth layer in water electrolysis under microgravity. *J. Electrochem. Soc.* **153,** E138 (2006).
33. H. Cheng, K. Scott, and C. Ramshaw: Intensification of water electrolysis in a centrifugal field. *J. Electrochem. Soc.* **149,** D172 (2002).
34. S. Kim, N. Koratkar, T. Karabacak, and T.M. Lu: Water electrolysis activated by Ru nanorod array electrodes. *Appl. Phys. Lett.* **88,** 263106 (2006).
35. P.C. Chen, Y.M. Chang, P.W. Wu, and Y.F. Chiu: Fabrication of Ni nanowires for hydrogen evolution reaction in a neutral electrolyte. *Int. J. Hydrogen Energy* **34,** 6596 (2009).